Additive Manufacturing 70 (2023) 103578

Contents lists available at ScienceDirect

Additive Manufacturing

journal homepage: www.elsevier.com/locate/addma

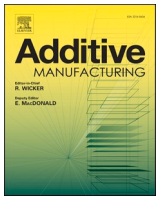

Electron-optical observation of smoke evolution during electron beam powder bed fusion

Jihui Ye [a,b,*], Jakob Renner [b], Carolin Körner [a,b], Zongwen Fu [a]

[a] Institute of Advanced Materials and Processes (ZMP), Friedrich-Alexander University Erlangen-Nürnberg, Dr.-Mack-Str. 81, 90762 Fürth, Germany
[b] Department of Material Science and Engineering, Friedrich-Alexander University Erlangen-Nürnberg, Martensstr. 5, 91058 Erlangen, Germany

ARTICLE INFO

Keywords:
Electron Beam Powder Bed Fusion (PBF-EB)
Smoke effect
Electron optical process monitoring

ABSTRACT

Electron Beam Powder Bed Fusion (PBF-EB) is an additive manufacturing technique that produces customized components using an electron beam under vacuum conditions. A so-called smoke phenomenon might occur during the process, leading to an explosion-like powder spreading in the vacuum chamber, which is catastrophic for the build process. This phenomenon happens rapidly and it is hard to be observed from its initial stage. In this study, the powder smoke phenomenon and its development are investigated using an ELectron-Optical (ELO) monitoring system, which collects backscattered electrons during PBF-EB in similarity to scanning electron microscopy. In comparison to the optical process monitoring tool based on high-speed camera, the ELO system shows very promising results for real-time smoke detection and possibly prevention.

1. Introduction and conceptualization

Since the first successful flight of the new Boeing 777X equipped with a GE9X engine containing titanium aluminide turbine blades fabricated by means of Electron Beam Powder Bed Fusion (PBF-EB) in 2020, the PBF-EB technology attracts increasing research interest [1,2]. However, PBF-EB still finds limited industrial application in comparison with its sister technology (i.e., the more mature Laser Powder Bed Fusion (PBF-L) process). One of the reasons is a lack of knowledge of the interaction between the electron beam and the powder particles [3]. A so-called powder smoking phenomenon can occur, causing an explosion-like powder spreading in the vacuum chamber and lowering the process stability [3,4]. So far, the smoke event is thought to result from an avalanche effect: at the beginning, a few particles are lifted into the vacuum and lose their electrical contact; subsequently, these lifted particles are further charged by the incident electron beam and are accelerated into the direction of the powder bed resulting in a catastrophic smoke event [2]. If the PBF-EB process could be promptly interrupted in the initial stage of powder smoking (particle lifting), the smoke event would be prevented and the PBF-EB process parameters could be appropriately adjusted.

Since the first successful flight of the new Boeing 777X equipped with a GE9X engine containing titanium aluminide turbine blades fabricated by means of Electron Beam Powder Bed Fusion (PBF-EB) in 2020, the PBF-EB technology attracts increasing research interest, especially in academics [1,2]. However, compared to its sister technology (i.e., the more mature Laser Powder Bed Fusion (PBF-L) process), PBF-EB, showing unique features, still finds limited industrial application due to deficient knowledge of the interaction between the electron beam and the powder particles [3]. In addition, under certain circumstances, an undesired powder smoking phenomenon can occur, causing an explosion-like powder spreading in the vacuum chamber and lowering the process stability [3,4]. So far, the smoke event is thought to result from an avalanche effect: at the beginning, a few particles are lifted into the vacuum and lose their electrical contact; subsequently, these lifted particles are further charged by the incident electron beam and are accelerated into the direction of the powder bed resulting in a catastrophic smoke event [2]. If the PBF-EB process could be promptly interrupted in the initial stage of powder smoking (particle lifting) the smoke event would be prevented and the PBF-EB process parameters could be appropriately adjusted.

Zäh et al. [5,6] used an optical high-speed camera to observe the smoke process generated with an electron beam standing still or drawing a circle; simultaneously, they also measured the specimen current (ground current) conducted by the steel build plate during the injection of the electron beam into the powder bed [6]. A sudden drop in the

* Corresponding author at: Institute of Advanced Materials and Processes (ZMP), Friedrich-Alexander University Erlangen-Nürnberg, Dr.-Mack-Str. 81, 90762 Fürth, Germany.
E-mail address: jihui.ye@fau.de (J. Ye).

https://doi.org/10.1016/j.addma.2023.103578
Received 14 December 2022; Received in revised form 21 April 2023; Accepted 22 April 2023
Available online 23 April 2023
2214-8604/© 2023 Elsevier B.V. All rights reserved.

specimen current was detected when a smoke event took place; i.e., during powder smoking, most of the electrons are scattered by moving powder particles above the specimen instead of forming specimen current [6]. In commercial PBF-EB machines, the Arcam company developed an x-ray sensor inside the electron beam column (above the build chamber) to detect the powder smoking in an early stage and to protect the cathode. In the course of the smoke event, powder particles in the build chamber can lift and diffuse into the electron beam column. Owing to the interaction (inverse photoelectric effect) between the electron beam and the lifted powder particles in the electron beam column, x-ray inside the electron beam column is generated and detected.

Among all different process monitoring approaches and smoke detection systems, ELectron-Optical (ELO) observation, which is not sensitive to any temperature effects and shows high accuracy, is thought to be one of the most promising in-situ monitoring techniques [2,7]. The principle of ELO imaging is comparable to Scanning Electron Microscopy (SEM) [8–10]. During ELO imaging, secondary electrons (SE) and backscattered Electrons (BSE) generated by the interaction between the incident electron beam and the powder bed are collected in the form of a current signal using detectors located above the powder bed [10]. The number of SE and BSE affects the ELO signal intensity; i.e., significant fluctuations of the ELO signal are observable, when the incident electron beam meets the flying powder particles resulting from the powder smoke event.

In this study, the ELO signals derived during the whole smoke event are analyzed. Shortly before the catastrophic smoke, abnormal fluctuations of the ELO signal are detected, which results from small local movements of powder particles observed using a high-speed camera. In addition, the evolution of the ELO signal related to the smoke event is discussed. The analysis of the ELO signal derived during PBF-EB offers the possibility to identify powder smoking at the early stages before the occurrence of a catastrophic smoke event.

2. Material and experimental methods

The experiments were conducted on a freely programmable PBF-EB machine: Freemelt ONE (Freemelt AB, Mölndal, Sweden). The machine operates with an acceleration voltage of 60 kV under a constant helium pressure of 10^{-3} mbar. Two process monitoring methods are applied, as illustrated in Fig. 1. An ELO imaging module with a centrally symmetric ring-shaped detector plate is located directly above the build area and coaxially with respect to the incident electron beam. The ring has a diameter of 140 mm and a work distance of 160 mm. It collects part of the reflected electrons during the process creating a negative voltage signal, which is then converted into a digital signal by a digitizer. ELO delivers continuous time-series data with a sampling rate of 250 kHz. At the same time, an optical high-speed camera (Sony r×100 v, Tokyo, Japan) with a frame rate of 500 frames per second is mounted outside of the vacuum chamber. The whole PBF-EB process is monitored using the high-speed camera through a viewport. Images taken by this camera are post processed using digital image correlation (DIC) [11] to better illustrate the changes in the powder bed. To be more specific, images are obtained by differentiating event images where the powder bed is unstable and a reference image with a calm powder bed. By registering the data from ELO system and high-speed camera, it is possible to compare the information derived from the two systems under the same time scale. However, the accuracy of data registration is not perfect due to different natures of the datasets. The ELO data is a time series data and high-speed camera captures are images. In addition, the Freemelt machine is equipped with an internal data logging system which records machine status in the background.

Properly setting up the experimental environment for smoke observation is crucial. First, it is important to ensure that the smoke event can be easily triggered. According to Cordero et al., smoke is highly related to the electrical properties of the powder bed, which are strongly influenced by temperature [4]. Therefore, for this study, a powder bed

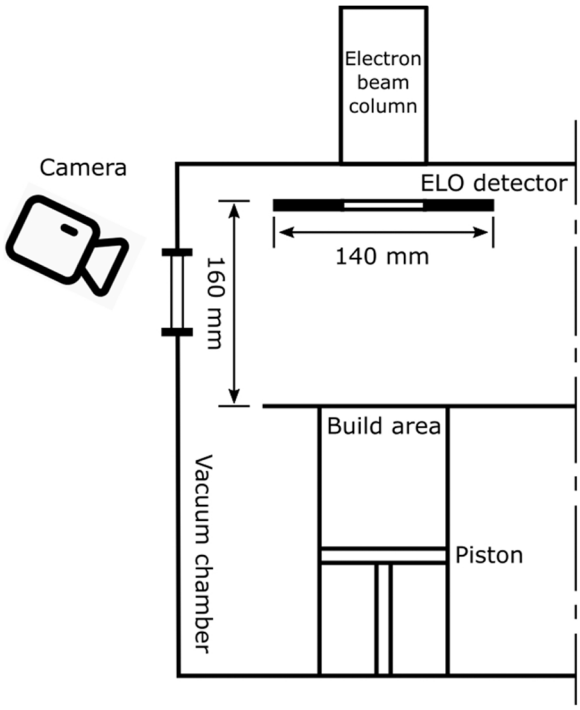

Fig. 1. Schematic illustration of the build chamber of the Freemelt ONE machine equipped with an ELO system and a high-speed camera.

temperature of 50 °C was selected. Second, the ELO signal should be generated from a uniform powder bed. Therefore, the applied powder layer thickness was kept at 500 μm, ensuring that the start plate was completely covered by powder particles. For a normal PBF-EB process, the layer thickness commonly varies between 50 μm and 100 μm, which usually results in a not fully covered build plate showing numerous uncovered void areas after powder raking; thus, ELO signals might show significant fluctuation when scanning the covered and uncovered area with different surface morphology and material types. Additionally, a stainless steel plate with a thickness of 20 mm and a diameter of 100 mm was chosen as the start plate. It was electrically grounded with a thermocouple attached to its bottom. The material chosen for this study is inert gas-atomized Ti-6Al-4V with a spherical particle shape (Ti-6Al-4V, ELI grade 23; particle size 45–105 μm, Macon, France).

The hatching strategy used in this study is a line-ordered pattern; a schematic pattern is shown in Fig. 2. This type of pattern is usually square shaped which is widely used for preheating to sinter loosely-packed powder particles in order to avoid the smoke event [12,13]. Three major factors determine such a hatching strategy: line offset L_{offset}; line order L_{order} and line length L_{line}. With the coordinate system defined in Fig. 2, the basic components of this pattern are straight hatching lines parallel to x-axis. These hatching lines are perpendicular to the y-direction and parallel to each other over the entire scanning area with a certain line offset. After scanning through one hatching line, the electron beam skips several lines in y-positive direction depending on line order. When there is no more hatching line in y-positive direction, the electron beam returns to the other side (y-negative direction) and scans the most initial no-scanned line. This procedure is repeated until all hatching lines are scanned.

For a better discussion in the following chapter, the consecutive scanned hatching lines before the electron beam returns to the other side are grouped as a **line set**. For example, the pattern shown in Fig. 2 has a line set consisting of twelve hatching lines. The exact hatching parameters for the examined line-ordered pattern are displayed in the diagram, where v_{beam} stands for beam scan speed. This pattern is repeated five times to ensure smoke event is triggered during preheating. The beam

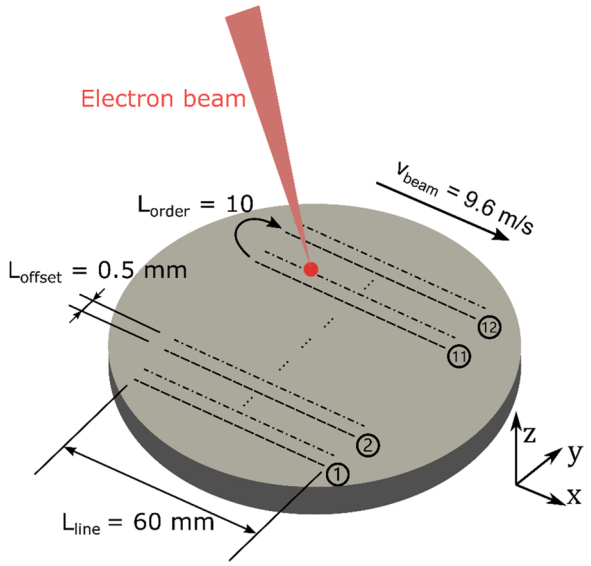

Fig. 2. Illustration of a line-ordered preheating pattern. Hatching lines marked from ① to ⑫ are hatched consecutively and they are grouped as a line set. The exact hatching parameters are shown in this image.

size is 500 μm with the definition from full width half power (FWHP), and beam power is not a constant value because the smoke happens before the target beam current is reached. Freemelt ONE uses a diode thermionic electron gun which requires a few hundreds of milliseconds of ramping time [2] to reach the target beam current. When executing the previously described hatching pattern, Freemelt ONE always scans the desired pattern while trying to reach the target current. And the smoke events are observed during the beam ramping phase. Therefore, triggering smoke with a clearly defined beam current is hard to realize under this circumstance.

3. Results

A smoke event was successfully triggered using the process parameters shown in Fig. 2. As mentioned in the previous section, the exact beam current triggering smoke is hard to be regulated due to the diode electron gun design. At the same time, the data logging system has a sampling rate of 3 Hz for beam current, which only allows a rough estimation of beam current when smoke event is triggered, which lies between 1 mA and 2 mA. Fig. 3a depicts ELO signal development from this smoke event. In addition, Fig. 3b shows post-processed high-speed camera images.

Most of other researchers focus on the smoke event generated from simple geometric patterns like a point or a circle [5,6]. The smoke event observed from this line-ordered pattern consists of three distinctive stages. At the beginning (**stage I** of Fig. 3a), the powder bed is calm, as illustrated in the capture taken ~700 ms (Fig. 3b_1). There are a few bright spots spreading over the field. They are noises created by high-speed camera. Subsequently (the boundary between **stage I & II** of Fig. 3a), a single powder fume appears along one hatching line at ~780 ms (Fig. 3b_2). This powder fume differs from a catastrophic smoke event with its size. It is generated from a local powder explosion event, which does not escalate, and self-recovers over time. Afterwards (**stage II** of Fig. 3a), more and more similar powder fumes form as the beam continue hatching. The capture from ~930 ms (Fig. 3b_3) shows four powder fumes along the current hatching line. At the same time, some powder fumes from previous hatching lines are still active in this image. At ~1100 ms (Fig. 3b_4 and **stage III** of Fig. 3a), a big powder fume is created where a conventionally defined catastrophic smoke event happens.

Fig. 3a demonstrates the corresponding ELO signal from this smoke event. In **stage I** and **II** of Fig. 3a, the signal intensity continuously increases due to beam current ramping. At the end (**stage III** of Fig. 3a), a

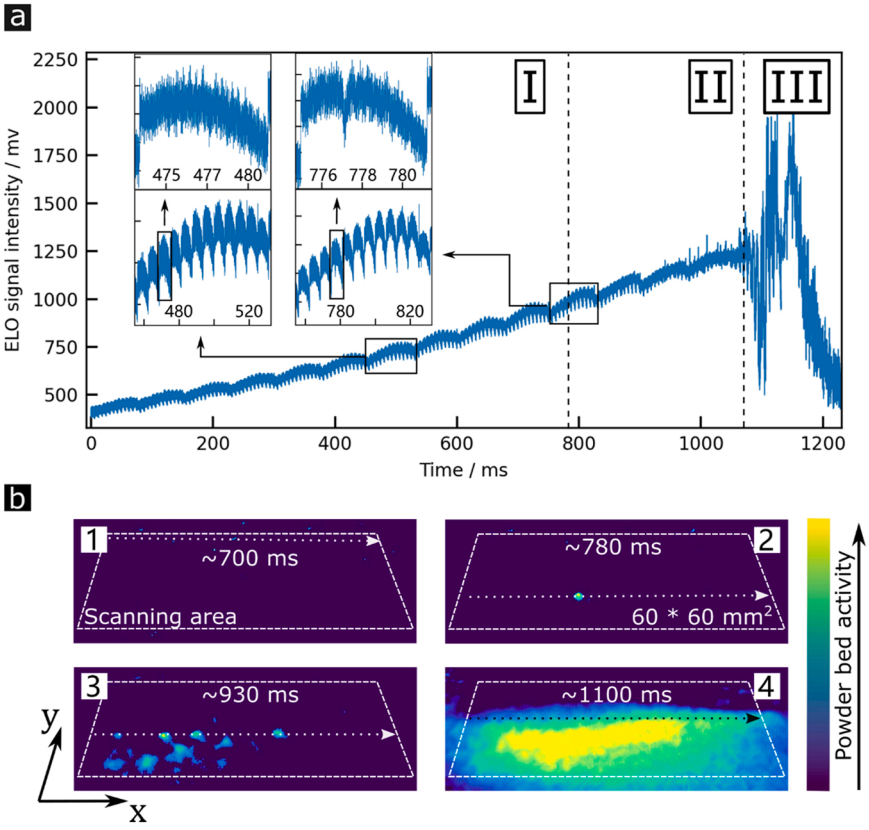

Fig. 3. (a):ELO signal development during a smoke event. The signal is periodic because of hatching pattern, where the minor cycle is a result of hatching lines and major cycle is created by line sets. Three characteristic stages are determined based on the noise level as well as high-speed camera result. Stage I: stable period without noticeable abnormal signal fluctuation(1st to 10th line sets); stage II: unstable period, in which small local powder fumes and abnormal fluctuations of the ELO signal are observed(11th to 14th line sets); stage III: a catastrophic smoke event leading to chaotic ELO signal(15th line set). Four insets show more details about the signal evolution. (b_1 – b_4): High-speed camera images recorded during this smoke event. These images are obtained by differentiating event images where the powder bed is unstable and a reference image with a calm powder bed. The dotted lines mark the position and direction of the actual hatching line when these images are taken. The colorbar on the right represents the difference in intensity, which can be regarded as the powder bed activity. The bright spots over the scanning area are mostly powder fumes.

big fluctuation initiates at 1070 ms. Four insets reveal more details about this development. The inset from 460 to 520 ms shows a representative signal development from the 7th line set. Here, twelve similar curves are observed with each of them standing for ELO signal from one hatching line in that line set. The general tendency of ELO signal intensity from these twelve hatching lines first increases and then slightly decreases. Another inset from 475 to 480 ms illustrates the signal development from the 6th hatching line from that line set. The signal forms an arch shape with heavy noises. This kind of signal development pattern continues until 780 ms, where an abnormal signal fluctuation appears as the electron beam hatches the 4th hatching line in the 11th line set, as depicted in the inset from 776 to 780 ms. The appearance of this abnormal fluctuation marks the transition of ELO signal from **stage I** to **II.** In the meanwhile, the inset from 770 to 820 ms shows the ELO signal from that line set. It has a similar signal development as previous line sets. After the observation of this abnormal signal fluctuation, more and more similar fluctuations are observed in ELO signal until the signal enters a totally chaotic stage, **stage III**.

4. Discussion

4.1. Smoke development

Judging from high-speed camera captures, the smoke event triggered from this line-ordered pattern has three characteristic stages. **Stage I**: a stable stage (Fig. 3b$_1$), **stage II**: a meta stable powder fume development stage (Fig. 3b$_2$ & b$_3$) and **stage III**: a catastrophic powder avalanche stage (Fig. 3b$_4$). The powder bed is calm in the stable stage. The appearance of powder fume marks the transition from **stage I** to **stage II**. The authors assume that the spreading of charged particles is likely the key for powder fume propagation. The charged powder particles jump up from one local spot and fall down in a neighbouring area. The spreading of charged powder particles could trigger more powder fumes when the neighbouring area is radiated by electron beam again. In this way, more and more powder fumes appear as the electron beam continues hatching in **stage II**. In the end, when the density or the intensity of powder fumes exceeds a certain threshold, a catastrophic powder avalanche happens. The different stages and the smoke development observed using ELO and high-speed camera are in good accordance with each other. This observation matches the stage-wise smoke development model reported by Wang et al. [14].

Furthermore, 173 other process parameter combinations (varying v_{beam}, L_{offset}, L_{order} and beam size) were conducted. The majority of catastrophic powder smoking follows the same pattern where small local powder fumes cause the avalanche effect. Nevertheless, the formation mechanism of the local powder fumes is unclear and will be further investigated in future work.

4.2. ELO monitoring smoke event

The general development of ELO signal during hatching is clear. In Fig. 3a, the gradual increase in ELO signal is a result of the ramping up beam current [2]. In addition, the ELO signal intensity can be affected by following aspects. As the beam moves from one side of scanning area to the other side, the distance between the impact point and the detector plate first decreases as the beam approaches the middle point and then increases when the beam moves away. The variation in the distance creates first an increase and then a decrease solid angle, which is the amount of field of view from impact point that the detector plate covers, as shown in Fig. 4. This solid angle variation creates a first increase then decrease ELO signal trend. Such trend can be found not only within one hatching line (when beam moves towards positive x-direction) but also within one line set (when beam moves towards positive y-direction between hatching lines). Another aspect is the signal local fluctuation caused by surface morphology, the random distribution of powder particles forms a uneven morphology, which contributes a certain noise to the signal. At last, the amplifier from signal chains adds additional noise to ELO signal.

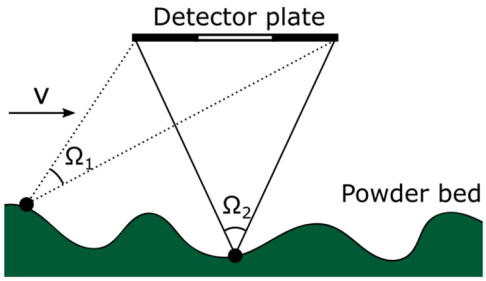

Fig. 4. Illustration of solid angle variation due to electron beam movement. As the electron beam moves from left to right, the general solid angle first increases then decreases. In the meanwhile, the powder bed is not perfectly even, a rough morphology creates additional fluctuating solid angle to the general trend.

The correlation between the evolution of the smoke event and the ELO signal can be better understood when previous mentioned influences are removed. Therefore, the original ELO data was post-processed using the method shown in Fig. 5. Fig. 5a is an exemplar of the ELO signal from the 11th line set, where twelve dashed lines slice the signal into sections based on hatching lines. In Fig. 5b, each signal section was subtracted with its 2nd degree polynomial fitted curve in order to eliminate the influence introduced by the solid angle variation. Thus, flat ELO data curves were derived, as depicted in Fig. 5c. Subsequently, a low-pass-filter with a cut-off frequency of 20 kHz [15] was applied to the processed data to remove the noise from the amplifier. According to Nyquist–Shannon sampling theorem [16], the highest detectable signal frequency after filtering will be limited to 10 kHz. Together with v_{beam} given in Fig. 2, any changes on powder bed which is longer than 0.96 mm can still be detected. Fig. 5d shows a post-processed signal section focusing on the interaction between the electron beam and the powder bed.

High-speed camera images from twelve hatching lines in 12th line set during the metastable powder fume development stage are plotted in Fig. 6. Bright spots in the post-processed images are active powder fumes after the electron beam finishes the current hatching line. Corresponding post-processed ELO signals are plotted beneath each capture. Additionally, grey ELO signal curves from 10th line set are plotted as reference, which represents the signal development during the stable stage. In general, the reference signal curves are more smooth and fluctuate around signal zero. Slight vibrations in reference signal are related to many factors, such as surface morphology or moving particles under the electron beam. An exact explanation on fluctuations in post-processed ELO signal is still unclear and it will be further studied in the future work.

As shown in Fig. 6, powder fumes are found in 3rd, 4th, 5th, 6th and 8th hatching lines from the 12th line set. In the meanwhile, abnormal ELO signal fluctuations are observed almost at the same location of powder fumes. These fluctuations are named as registered fluctuations for a better discussion. It is noticeable that all local powder fumes observed by means of the optical camera correspond to a decrease in ELO signal. The authors assume that the changing in powder local packing density during the occurrence of powder fume causes a reduction in ELO signal intensity. Powder bed locally expands when the powder fume forms so that part of the electrons have to go through more reflections before leaving the same area. Therefore, a decrease in ELO signal is expected.

In addition, some hatching lines (e.g., 1st, 4th, 6th, 8th, 9th and 11th hatching lines) showed abnormal fluctuations in the ELO curves, while the corresponding powder fumes were barely detectable according to optical images. These fluctuations are unregistered fluctuations. From

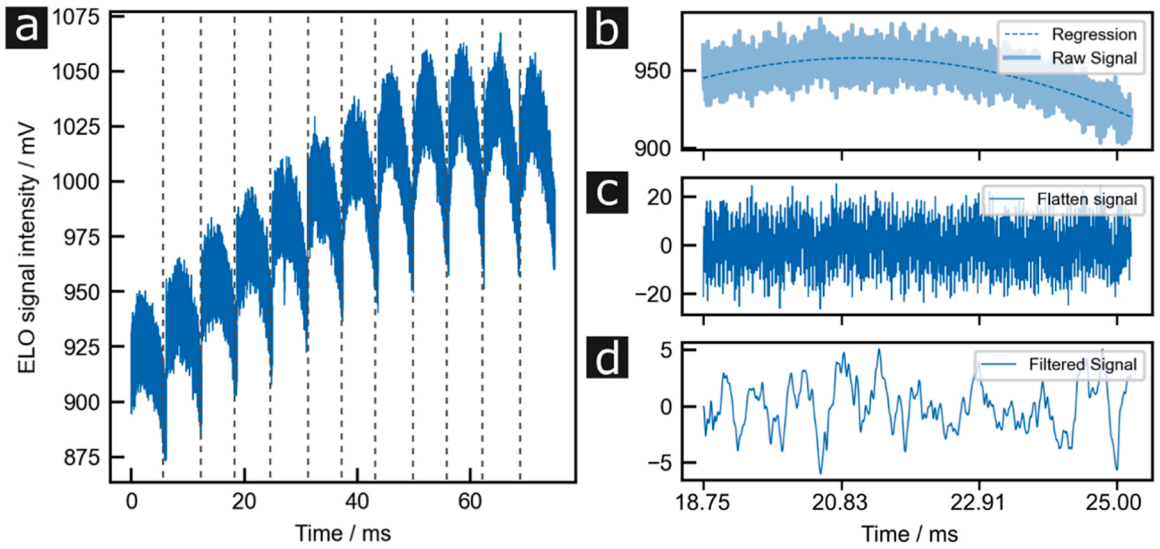

Fig. 5. (a):ELO signal from the 11th line set. Dashed lines separate the signal into sections based on hatching lines. (b):Solid angle correction. The ELO signal sections were subtracted with its fitted polynomial curve, which represents the solid angle variation introduced by electron beam movement.(c):Flattened signal after solid angle correction. (d):Noise correction. A low-pass filter was applied to eliminate the high-frequency noise introduced by amplifier.

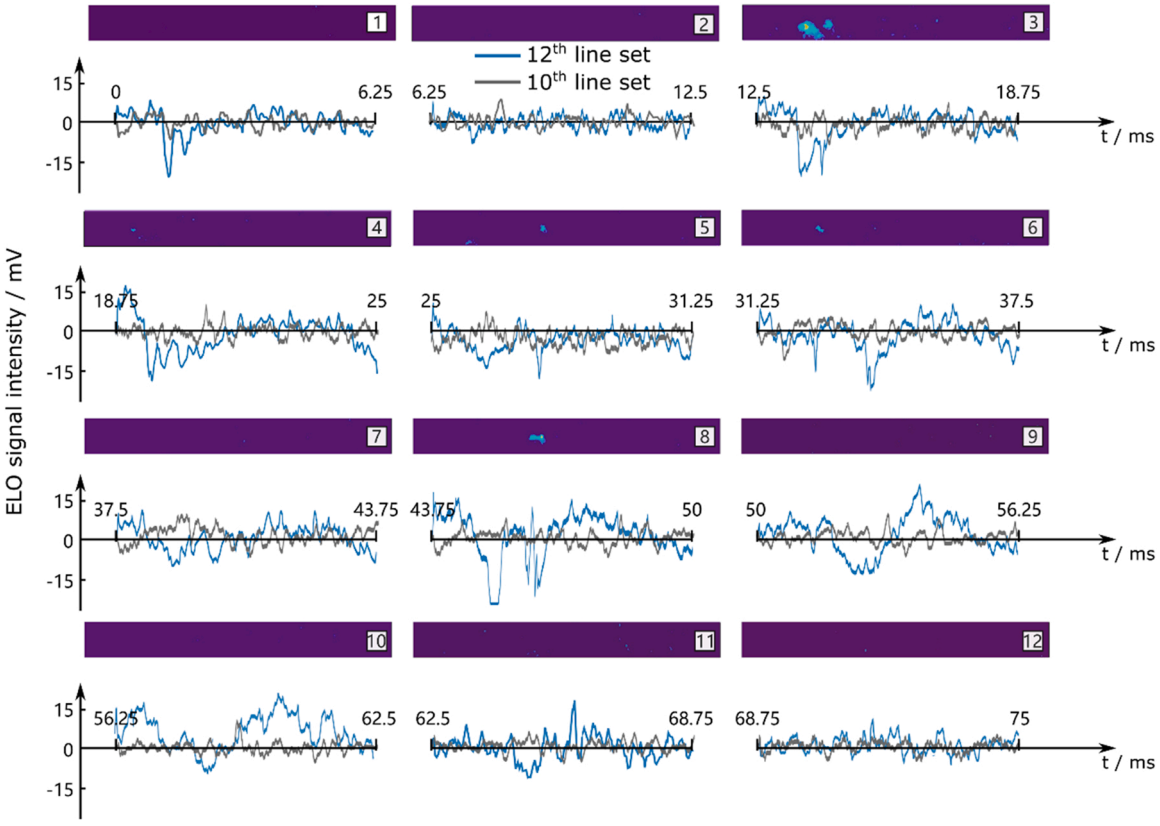

Fig. 6. Comparison between high-speed camera and ELO system. Post-processed high-speed camera images related to twelve consecutive hatching lines from the 12th line set are presented. These images are taken after the electron beam has finished current hatching line. Their corresponding post-processed ELO signal sections are displayed in blue color. Grey ELO signal curves represent signal development from a stable stage, which is generated from the 10th line set.

the authors' point of view, some slight mismatch between the ELO signal and the optical observation could be explained by the limited frame rate and the resolution of the high-speed camera used in this work. In the 1st hatching line, there could be a minor powder fume triggered on sight. However, the powder fume is not observable due to the limited resolution of the high-speed camera. In the 4th hatching line, unregistered fluctuations locate near the position of powder fumes from the 3rd hatching line. It is considered that part of the powder particles of powder fumes in 3rd hatching line expand faster in the y-positive direction than the electron beam moves between hatching lines, these airborne particles could influence the signal. At the same time, these particles are hardly detectable using the high-speed camera. The same assumption could also explain the unregistered fluctuations observed in the ELO curves for the 6th and 9th hatching lines. It should be noted that these

fluctuations are generally broader than the registered fluctuations from previous lines, which implies an expansion of powder fume in x-direction. However, a strong unregistered fluctuation is observed from the 8th hatching line but still no powder fume observable. In addition, several unregistered fluctuations that corresponds to a ELO signal increase are observed in 4th, 8th, 9th, 11th hatching lines. These two phenomena cannot be explained now and will be further studied. The discussion above indicates that the ELO system is more sensitive to powder bed activities and it contains more information in comparison to the high-speed camera.

Similar comparisons are performed throughout the ELO signal development during the smoke event. It is concluded that the ELO system is capable of locating most of the powder fumes as soon as they initiate. Additionally, the big ELO signal fluctuation from **stage III** is also proven to relate to the catastrophic powder avalanche.

Fig. 3 illustrates a stage-wise ELO signal development where the boundary is drawn mainly based on the observation of the high-speed camera. As previously discussed, the ELO system is generally more sensitive to changes within the powder bed in comparison to the high-speed camera. Fig. 7 further exploits the ability of the ELO system regarding the early detection of smoke event. The authors chose the fluctuation range of ELO signal from individual hatching lines as a feature for further analyzation, which can well present the calmness of the powder bed. The fluctuation range R_i is defined as the difference between the maximum I_{max} and the minimum I_{min} ELO signal intensity from a post-processed ELO signal section for i^{th} hatching line, as illustrated in Eq.(1). For example, Fig. 5d is a post-processed ELO signal section from the 3rd hatching line in 11th line set, which has a fluctuation range value of 11 mV.

$$R_i = I_{max} - I_{min} \tag{1}$$

Such fluctuation range values from all ELO signal sections are plotted in Fig. 7. In the meanwhile, the smoke-onsets (observing the first powder fume event) derived from high-speed camera are plotted as grey dashed lines.

The fluctuation range in Fig. 7a develops with a period of twelve data points that corresponds to the number of hatching lines within one line set. Under this circumstance, a moving average (dashed blue curve) is calculated for a better illustration of fluctuation range development, which is a series of averages from previous twelve data points. The moving average stays stable in the beginning and then rapidly increases as smoke event develops. It is proven in Fig. 6 that powder movements increase the fluctuation in ELO signal. Therefore, the rapid increase in moving average indicates more and more powder starts moving on scanning area, which increases the instability of powder bed and eventually leads to a catastrophic smoke event. In comparison to the smoke onset derived from the high-speed camera that locates around 780 ms, fluctuation range shows some anomalies ahead of this time. Two red circles mark two possible smoke onsets that could be derived from the fluctuation range. The first circle marks one abnormal data point, which lies far away from the moving average line. The second circle focuses on the fluctuation range development within one line set which has a sparser distribution in comparison to previous ones. The same comparison is conducted in another smoke experiment varying v_{beam}, as shown in Fig. 7b. The general fluctuation range development is similar to the previous experiment and some anomalies from the fluctuation range can also be found ahead of the smoke onset derived from the high-speed camera.

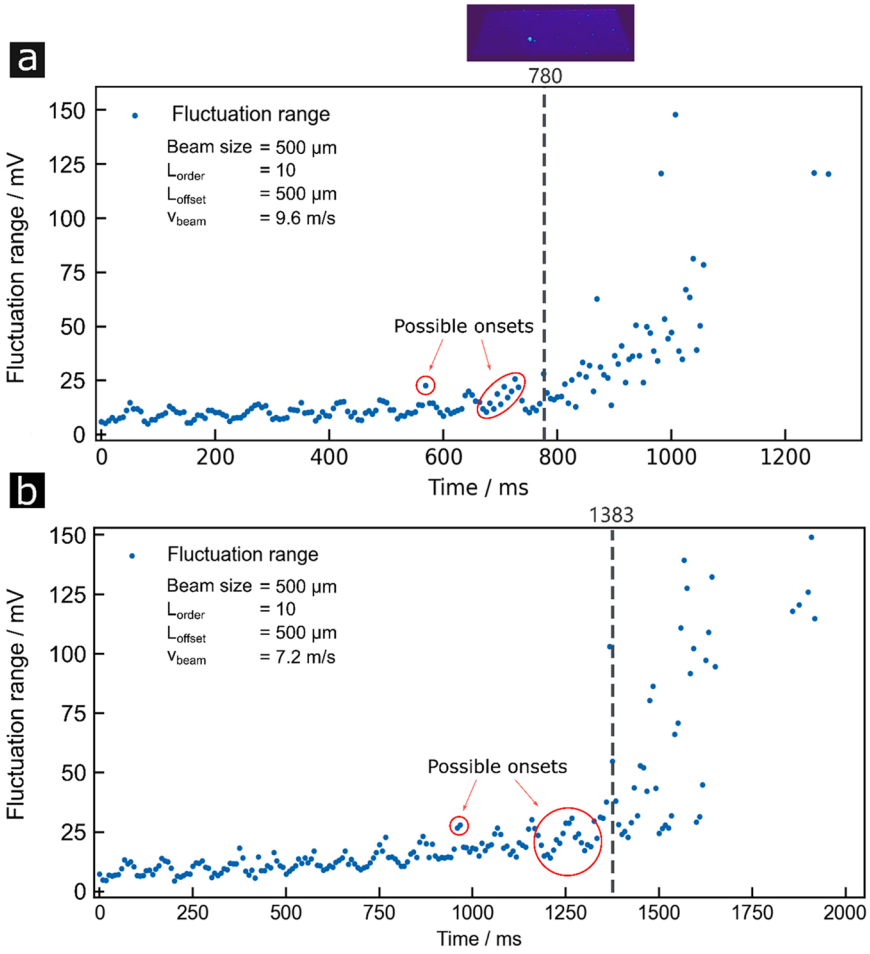

Fig. 7. Fluctuation range development of the ELO signal during smoke event evolution. Fluctuation range is calculated from each post-processed ELO signal section. Blue dashed curves are moving average, which is a series of averages from twelve previous data points. Grey lines are smoke onsets derived from high-speed camera (boundaries between stage I & stage II, dashed line). Red circles mark possible anomalies found in the fluctuation range.(a): Fluctuation range development from a smoke event triggered with the hatching parameter illustrated in Fig. 2. (b): Fluctuation range development from another smoke event with different v_{beam}.

To be noted, the possible smoke onsets (anomalies) found in the fluctuation range need to be further verified because they could also be false alarms. However, the validation will be performed in future study.

In comparison to the high-speed camera used in this study, the ELO system could be generally more sensitive to initial smoke events. This sensitivity is primarily due to the interaction between the electron beam and the flying particles. Although the authors used only one type of powder in the study, it can be assumed that the ELO system is capable of capturing smoke initial events from other feedstock. When switching to another feedstock, two major physical properties change: the chemical composition and particle size distribution of the feedstock material. The chemical composition determines the backscattered coefficient, with Inconel 718, for example, having a higher atomic number than Ti6Al4V resulting in a higher backscattered coefficient. This means that one can expect a higher ELO signal intensity from this powder and a higher signal-to-noise ratio, allowing for better identification of initial smoke events. On the other hand, particle size distribution mainly affects smoke sensitivity. The initial event can still be detected when the powder particles are lifted and block the electrons.

Moreover, the ELO system is a very robust monitoring tool as it is located in the vacuum chamber directly above the build area, where working conditions are extreme. The detector plate undergoes constant impact from electrons, x-rays, metallization, and flying particles but still delivers reliable signals.

In conclusion, using the ELO system as a monitoring tool for smoke event detection shows great promise.

5. Conclusion

In this study, smoke events triggered by a line-ordered hatching pattern in Electron Beam Powder Bed Fusion (PBF-EB) process were monitored using an ELectron Optical system (ELO) as well as a high-speed camera. According to high-speed camera capture, the smoke development can be separated into a stable stage, a meta stable powder fume development stage as well as a catastrophic powder avalanche stage. The ELO system is capable of capturing all these three stages. This opens up the possible application for ELO system as a very robust smoke monitoring tool at the initial stage.

CRediT authorship contribution statement

Jihui Ye: Writing – original draft, Visualization, Software, Methodology, Investigation, Conceptualization. **Zongwen Fu:** Writing – review & editing, Writing – original draft, Supervision, Resources, Project administration, Funding acquisition. **Jakob Renner:** Writing – review & editing, Software, Conceptualization. **Carolin Körner**: Writing – review & editing, Supervision, Resources, Project administration, Funding acquisition.

Declaration of Competing Interest

The authors declare the following financial interests/personal relationships which may be considered as potential competing interests: Jihui Ye reports financial support was provided by Deutsche Forschungsgemeinschaft (DFG).

Data Availability

The authors do not have permission to share data.

Appendix A. Supporting information

Supplementary data associated with this article can be found in the online version at doi:10.1016/j.addma.2023.103578.

References

[1] B. Blakey-Milner, P. Gradl, G. Snedden, M. Brooks, J. Pitot, E. Lopez, M. Leary, F. Berto, A. du Plessis, Metal additive manufacturing in aerospace: a review, Mater. Des. 209 (2021), 110008.
[2] Z. Fu, C. Körner, Actual state-of-the-art of electron beam powder bed fusion, Eur. J. Mater. 2 (1) (2022) 54–117.
[3] C.P. Paul, A.N. Jinoop, A. Kumar, K.S. Bindra, Laser-based metal additive manufacturing: technology, global scenario and our experiences, Trans. Indian Natl. Acad. Eng. 6 (4) (2021) 895–908.
[4] Z.C. Cordero, H.M. Meyer, P. Nandwana, R.R. Dehoff, Powder bed charging during electron-beam additive manufacturing, Acta Mater. 124 (2017) 437–445.
[5] M. Zäh, M. Kahnert, Den Elektronenstrahl für das selektive Sintern von metallischen Pulvern nutzen, Euro-uRapid2006; Frankfurt/Main 27(28.11), 2006.
[6] C. Eschey, S. Lutzmann, M. Zaeh, Examination of the powder spreading effect in Electron Beam Melting (EBM), Solid Free. Fabr. (2009) 3–5.
[7] M.L.G. Grasso, A. Remani, A. Dickins, B.M. Colosimo, R.K. Leach, In-situ measurement and monitoring methods for metal powder bed fusion–an updated review, Meas. Sci. Technol. (2021).
[8] C.R. Pobel, C. Arnold, F. Osmanlic, Z. Fu, C. Körner, Immediate development of processing windows for selective electron beam melting using layerwise monitoring via backscattered electron detection, Mater. Lett. 249 (2019) 70–72.
[9] C. Arnold, J. Böhm, C. Körner, In operando monitoring by analysis of backscattered electrons during electron beam melting, Adv. Eng. Mater. 22 (9) (2020), 1901102.
[10] D. Zhao, F. Lin, Dual-detector electronic monitoring of electron beam selective melting, J. Mater. Process. Technol. 289 (2021), 116935.
[11] M.A. Sutton, J.J. Orteu, H. Schreier, Image Correlation for Shape, Motion and Deformation Measurements: Basic Concepts, Theory and Applications, Springer Science & Business Media, 2009.
[12] C.L.A. Leung, R. Tosi, E. Muzangaza, S. Nonni, P.J. Withers, P.D. Lee, Effect of preheating on the thermal, microstructural and mechanical properties of selective electron beam melted Ti-6Al-4V components, Mater. Des. 174 (2019), 107792.
[13] C.J. Smith, S. Tammas-Williams, E. Hernandez-Nava, I. Todd, Tailoring the thermal conductivity of the powder bed in Electron Beam Melting (EBM) Additive Manufacturing, Sci. Rep. 7 (1) (2017) 10514.
[14] D. Wang, D. Zhao, X. Liang, X. Li, F. Lin, Multiple stages of smoking phenomenon in electron beam powder bed fusion process, Addit. Manuf. 66 (2023), 103434.
[15] S. Butterworth, On the theory of filter amplifiers, Wireless Eng. 7 (6) (1930) 536–541.
[16] C.E. Shannon, Communication in the presence of noise, Proc. IRE 37 (1) (1949) 10–21.